Abnormal Infrared Effects of Nanostructured Rhodium Thin Films for CO Adsorption at Solid/Gas Interfaces

Wen-Guang Lin, Shi-Gang Sun,* Zhi-You Zhou, Sheng-Pei Chen, and Han-Chun Wang

State Key Lab for Physical Chemistry of Solid Surfaces, Department of Chemistry, Xiamen University, Xiamen 361005, China

Received: April 9, 2002; In Final Form: June 9, 2002

Nanometer-scale thin films of rhodium supported on glassy carbon (nm-Rh/GC) were prepared by electrochemical deposition using cyclic voltammetry. STM studies demonstrated that the Rh film is made of layered crystallites of an average size 230 nm (l) × 90 nm (w) × 10−30 nm (h). In situ FTIR spectroscopic investigations revealed, for the first time, that the nanostructured film exhibits abnormal infrared effects (AIREs) for CO adsorption at solid/gas interfaces. The AIREs are characterized by the inverting of the direction of IR bands of adsorbed CO (CO_{ad}), an enhancement of IR absorption intensity, and an increase in the full width at half-maximum (FWHM) of the bands. The inversion of the direction of the absorption bands and the increase in the FWHM are observed in spectra of CO on nm-Rh/GC of different Rh film thicknesses; the enhancement of IR absorption depends strongly on the thickness of the Rh film. The maximum enhancement factor has been determined to be 10.38 for an Rh film thickness of 79 nm. The present study demonstrated that the AIREs are general phenomena exhibited by nanostructured thin-film materials at both solid/liquid and solid/gas interfaces; they are of importance in revealing the intrinsic properties of 2D nanomaterials.

Introduction

We have shown recently that IR absorption of CO or other molecules (e.g., SCN^-, poly(*o*-phenylenediamine) (PoPD), etc.) adsorbed on electrodes of nanostructured thin films of the platinum-group metals (Pt, Pd, and Ru) and alloys (PtPd, PtRu) at solid/liquid interfaces produce abnormal IR features.[1−9] In comparison with the IR features of CO adsorbed (CO_{ad}) on electrodes of the corresponding massive metals, the abnormal IR features have three characteristics: (1) inverting of the direction of the CO_{ad} band; (2) enhancement of the IR absorption intensity; and (3) an increase in the full width at half-maximum (FWHM) of the CO_{ad} band. These abnormal IR features appear to be characteristics of nanometer-scale films and depend mainly on the structure and thickness of the thin film. We have proposed to nominate the phenomena as abnormal infrared effects (AIREs)[6] to differentiate them from so-called surface-enhanced IR absorption (SEIRA).[10−12] The latter describes the phenomenon of enhancement of IR absorption by *p*-nitrobenzoic acid (PNBA) and molecules of a similar structure[10,11] or by CO[12] molecules that are adsorbed on films of the coinage metals (mainly Au and Ag) having an island structure. The difference in the IR features of AIREs and SEIRA consists mainly of the inversion of the direction of the IR bands of the adsorbates. AIREs have also been confirmed for nanometer thin films of Ir,[13] Os,[14] and platinized platinum[15] in studies on solid/liquid interfaces.

As a member of the platinum-group metals, rhodium and its alloys exhibit a high activity[16,17] and have been commonly used for the simultaneous conversion of nitrogen oxides, carbon monoxide, and hydrocarbons in catalytic converters of automobile exhaust.[18,19] In addition, Rh compounds are also well known as highly effective chiral catalysts.[20] Different kinds of Rh materials such as poly- and single-crystal rhodium,[21−33] highly dispersed Rh,[34,35] and Rh clusters or particles supported on substrates[36,37] have been extensively investigated for CO adsorption not only at solid/liquid interfaces but also at solid/gas interfaces and in high-vacuum environments. It is known from these investigations that CO is adsorbed on Rh, yielding normally linearly bonded CO (CO_L, 2090−2000 cm^{-1}) and bridge-bonded CO (CO_B, 2000−1900 cm^{-1}) species. Recently, the study [38] of Rh thin films deposited on various substrates has attracted considerable attention for the purpose of developing effective catalytic materials.

In this paper, nanometer thin films of Rh were prepared by electrochemical deposition. The Rh films were characterized by scanning tunneling microscopy in the atmospheric environment and by cyclic voltammetry. CO adsorption was employed as a probe reaction. Together with in situ Fourier transform infrared reflection spectroscopy, the abnormal infrared properties of the Rh thin films have been revealed. The present study has extended the AIREs of platinum-group metals and alloys discovered previously at solid/liquid interfaces to solid/gas interfaces; emphasis has been placed on elucidating the dependence of the AIREs on the Rh film thickness (i.e., the size of 2D Rh film nanomaterial).

Experimental Section

Preparation of Nanostructured Thin Films of Rhodium. Thin films of rhodium were prepared by electrochemical deposition of Rh, under cyclic voltammetric conditions, onto a glassy carbon (GC) substrate 6 mm in diameter (the geometric area $A_{GC} = 0.28$ cm^2). The GC substrate was sealed into Teflon and polished mechanically by successively using sand paper and alumina powder of sizes 5, 1, 0.3 and 0.05 μm. The electroplating solution contains 0.1 M H_2SO_4 and 5.0×10^{-3} M Rh^{3+} ions. For deposition, the lower and upper potential limits

* Corresponding author. E-mail: sgsun@xmu.edu.cn. Fax: +86 592 2183047.

10.1021/jp025917u CCC: $22.00
Published on Web 10/23/2002

in cyclic voltammetry were respectively −0.25 and 0.4 V (vs SCE), and the sweep rate was 50 mV s^{-1}. The thickness of the Rh film was controlled by varying the number of cycles in the voltammetry. The nanometer-scale thin film of Rh prepared using the above procedure is designated as nm-Rh/GC(n), with n being the number of cycles. An EG&G potentiostat/galvanostat (model 263A) was employed in the electrochemical studies. A saturated calomel electrode (SCE) served as reference electrode.

In Situ Fourier Transform Infrared Spectroscopy. In situ FTIR spectroscopic studies were carried out using a Nexus 870 spectrometer (Nicolet) that is equipped with a liquid-nitrogen-cooled MCT-A detector and an EverGlo™ IR source. An electrochemical IR cell having a thin layer configuration[39] was employed in studies of solid/gas interfaces. A CaF_2 disk was used as an IR window, and the Rh thin film supported on GC was pushed against the window to form a thin cavity (the space between the IR window and the Rh film) during FTIR measurements. The infrared radiation from the IR source passed through the CaF_2 window and the thin cavity and reflected from surface of the Rh thin film.

The procedure for obtaining in situ FTIR spectra was as follows: (1) after optical alignment, the background single-beam reflectance spectrum (R_b) was collected with pure N_2 gas in the cell; (2) by fixing the same thin cavity between the Rh thin film and the CaF_2 window, the IR cell was filled with CO gas of high purity. The sample single-beam reflectance spectrum (R_s) was then recorded 5 min after CO gas was introduced into the cell in order to reach a saturation adsorption of CO on the Rh thin-film surface. The resulting spectrum was reported as absorbance (A) and was calculated from the equation

$$A = -\log \frac{R_s}{R_b} \qquad (1)$$

In the FTIR measurements, 400 interferograms were collected and co-added to obtain a single-beam spectrum; the spectral resolution was 2 cm^{-1}. According to the above experimental procedure and eq 1, IR absorption by both CO adsorbed on the Rh thin-film surface and gaseous CO in the thin cavity between the Rh thin film and the CaF_2 window will yield positive-going bands.

Scanning Probe Microscopy. A P4-SPM-18 scanning probe microscope (NT-MDT, Inc., Russia) was employed to study the microstructure and to measure the average thickness of Rh thin films in air.

Other Conditions. The nm-Rh/GC(n) was characterized by cyclic voltammetry in 0.1 M H_2SO_4, and the potential was cycled between −0.25 and 0.4 V at a scan rate of 50 mV s^{-1}. A polycrystalline rhodium film (geometric area $A_{Rh} = 0.27$ cm^2) was also characterized under the same conditions for comparison.

All solutions were prepared from superpure H_2SO_4 and ultrahigh-purity water obtained from Milli-Q lab equipment (Nihon Millipore Ltd.). The solutions were deaerated by bubbling high-purity N_2 gas through them before the measurement. All experiments were carried out at room temperature around 20 °C

Results and Discussion

1. Structure and Thickness of Rh Thin Films Investigated by Using a Scanning Tunneling Microscope. Figure 1 shows a typical STM image of the surface structure of nm-Rh/GC-(n = 10). It can be observed that the Rh thin film is composed

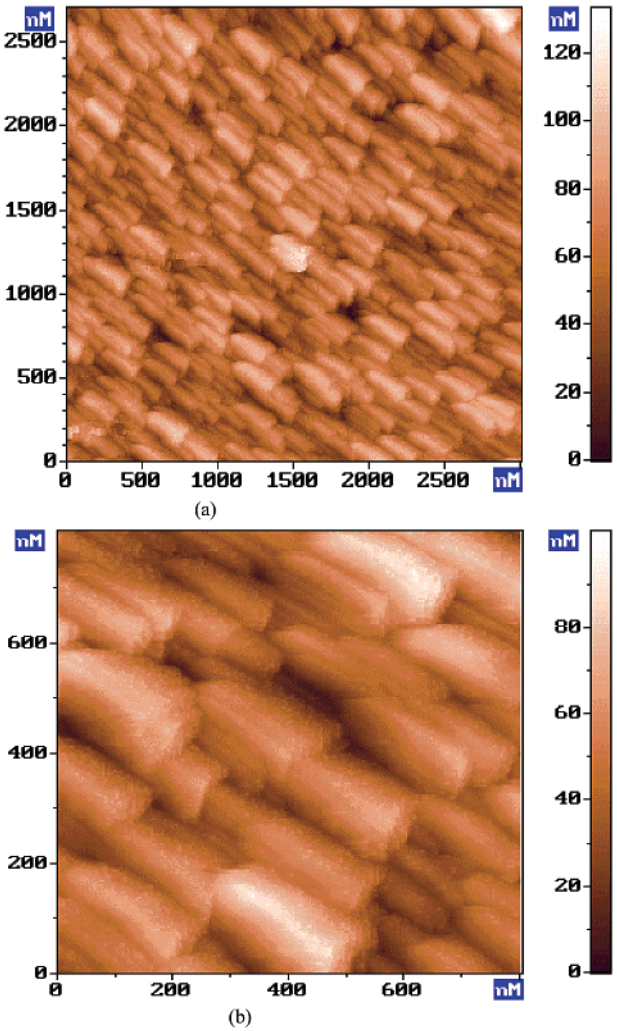

Figure 1. STM images of nm-Rh/GC(n = 10) prepared by electrodeposition from 0.1 M H_2SO_4 solution containing 5 mM Rh^{3+} ions: (a) V_b = 0.240V, I_t = 0.059 nA; (b) V_b = 0.320V, I_t = 0.029nA.

of layered Rh crystallites that appear in a rectangular form. Figure 1a shows that all Rh crystallites in the thin film are arranged in a defined direction. At higher magnification (Figure 1b), further details of the Rh crystallites can be clearly seen. It is interesting that the Rh crystallites in the thin film have almost the same size, which is around 230 nm (l) × 90 nm (w) × 10−30 nm (h) (Figure 1b). The structural characteristics of the Rh thin film in Figure 1 differ from those of Rh films prepared by electrodeposition at a fixed current density,[40] in which island crystallites of rhodium were formed. It is evident that the nanostructured Rh thin film has been generated from electrodeposition under cyclic voltammetric conditions; the electrodeposition under such conditions includes not only a nucleation process but also the diffusion-controlled growth of stable rhodium crystallites.[38]

The Rh thin film can be considered to be a kind of 2D nanomaterial.[41] The film is composed of nanometer-sized layers with a thickness that ranges from a few nanometers to a few hundreds nanometers. We estimate the thickness (d_e) of the film using following equation:

$$d_e = \frac{Q_d N_0 V_{Rh}}{3FA_{GC}74.05\%} \qquad (2)$$

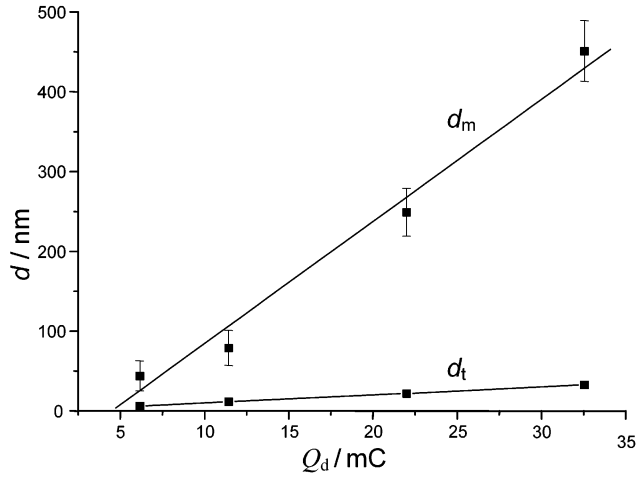

Figure 2. Relationship between Q_d and measured thickness (d_m) and calculated thickness (d_e) of Rh film.

Q_d is the electric charge consumed in electrodepositing Rh onto GC:

$$Rh^{3+} + 3e^- \rightarrow Rh \tag{3}$$

Q_d has been measured from the integration of $j-E$ curves recorded on electrodeposition; F is the Faraday constant, N_0 is Avogadro's number, V_{Rh} is the volume of one Rh atom ($V_{Rh} = {}^4/_3\pi r_{Rh}{}^3$), and A_{GC} is the geometric area of the GC substrate. The estimation of d_e according to eq 2 has been made by assuming that the efficiency of Rh is 100% and that the Rh atoms have cubic close packing to yield a space occupancy of 74.05%. The d_e calculated using eq 2 represents the thickness of the Rh thin film in which the electrodeposited Rh is packed in the same way as that of the massive Rh metal.

The thickness of thin-film materials can be also measured by using a scanning tunneling microscope, as described in our previous papers.[4,7] We have found that the Rh thin film can be eroded by applying a lithography voltage between the STM tip and the film. Because the threshold voltage to erode the Rh thin film (9.5 V) is smaller than that to corrode the GC substrate (about 11 V), a small hole will be drilled by the STM tip only on the Rh thin film when a lithography voltage below 11 V is applied. Once the bottom of the hole has reached the GC substrate, the average height of all pixels comprising the STM image can be taken as the measured average thickness (d_m) of the Rh thin film:

$$d_m = \frac{1}{n^2}\sum_{i=1}^{n}\sum_{j=1}^{n}|Z(i,j)| \tag{4}$$

where $|Z(i, j)|$ is the height measured starting from the GC substrate level of the pixel (i ,j) in the STM image and n^2 is the total number of pixels contained in the image. In the present study, $n = 256$, so a total of 65 536 pixels have been taken into account.

The variations of d_e and d_m with Q_d are compared in Figure 2. We can see that both d_e and d_m increase linearly with increasing Q_d. However, d_m is always larger than d_e at the same value of Q_d. The slope of the linear variation of d_m with Q_d was measured to be 15.8 nm mC^{-1}, which is much larger than that of d_e (1 nm mC^{-1}). This result implies that, as illustrated by STM images in Figure 1, the Rh crystallites are packed in a particular way in the thin film to form a layered nanostructure.

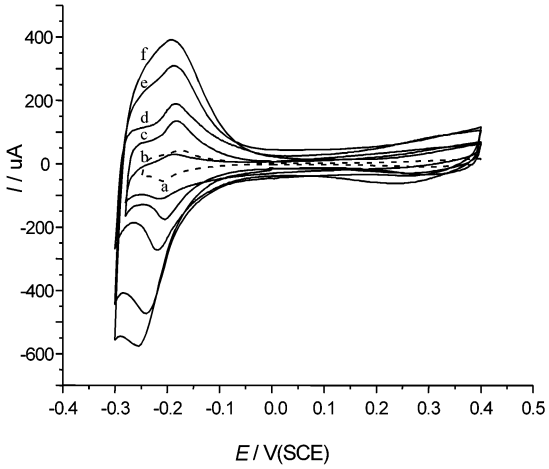

Figure 3. Cyclic voltammograms of Rh (a, dashed curve) and nm-Rh/GC(n) with $n = 4$ (b), $n = 10$ (c), $n = 15$ (d), $n = 30$ (e), and $n = 50$ (f) in 0.1 M H_2SO_4 solution with a sweep rate of 50 mV s^{-1}.

2. Electrochemical Characterization of Nanostructured Rh Thin Films. The Rh thin film was also characterized at solid/liquid interfaces by cyclic voltammetry using the adsorption/desorption of a hydrogen as probe reaction. Cyclic voltammograms obtained in 0.1 M H_2SO_4 solutions are shown in Figure 3. A voltammogram of a massive Rh electrode is also displayed in the Figure for comparison. In the potential region of hydrogen adsorption (−0.3 to 0.0 V), we observe a negative current peak near −0.21 V and a positive current peak near −0.17 V in the voltammogram of the massive Rh electrode. It is known[38,40,42] that these cyclic voltammetric (CV) features are due to the adsorption of hydrogen and anions and are characteristic of Rh surfaces. We observe similar CV features in voltammograms of nm-Rh/GC(n) electrodes with different Rh film thicknesses. However, when n is increased from 4 to 50, the intensity of both negative and positive current peaks increased gradually, and the peak potential shifts to more negative values. These results indicate that, following the increase of Rh film thickness, the surface roughness of nm-Rh/GC is increased accordingly because the geometric surface area of the GC substrate is constant (0.28 cm^2). In addition, the difference in peak potential (ΔE_p) between the negative and the positive current peaks increases with increasing n. ΔE_p is measured to be 26 mV for $n = 4$ and 57 mV for $n = 50$. The increase in ΔE_p implies that the adsorption process of hydrogen and anions on nm-Rh/GC surfaces becomes more and more irreversible as n increases. This is in accord with the results of Figure 2, which show that the porosity of the Rh thin film progressively increased with the increase in n (i.e., the growth of Q_d).

The relative surface roughness (R_r) of the Rh thin film is defined as the ratio of the geometric surface area of the Rh film to that of mechanically polished massive Rh. It can be calculated from a comparison of the charge density involved in hydrogen and ion adsorption processes on nm-Rh/GC with that on massive Rh:

$$R_r = \frac{Q_{CV}^{nm-Rh/GC}/A_{GC}}{Q_{CV}^{Rh}/A_{Rh}} \tag{5}$$

where $Q_{CV}^{nm-Rh/GC}$ and Q_{CV}^{Rh} are the electric charges involved in hydrogen and ion adsorption, respectively, on nm-Rh/GC and Rh and have been measured by integration of the corresponding voltammograms in the potential region of hydrogen adsorption; A_{GC} and A_{Rh} are the geometric areas of the GC substrate and

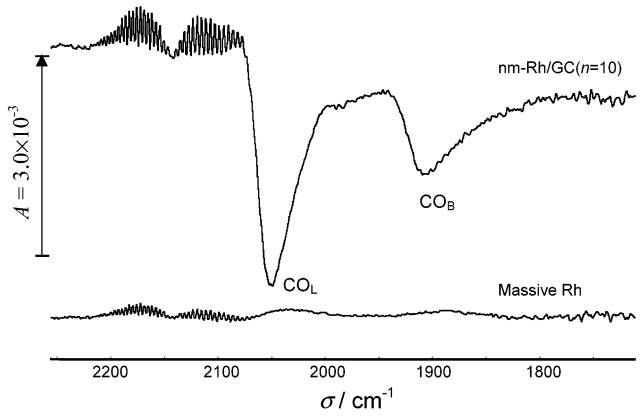

Figure 4. In situ FTIR spectra of gaseous CO and CO adsorbed on massive Rh and nm-Rh/GC($n = 10$) at solid/gas interfaces.

TABLE 1: Characteristic Parameters Derived from Cyclic Voltammetric Studies of Rh

Rh materials	Q_d/mC	d_e/nm	Q_{CV}/μC	R_r
massive Rh			293	1.00
nm-Rh/GC(n), $n = 4$	6.9	5.1	320	1.09
7	10.8	8.3	890	3.04
10	12.3	11.4	906	3.09
15	21.1	16.7	1376	4.70
30	33.3	32.5	2548	8.71
50	54.4	53.6	3383	11.56

massive Rh, respectively. The R_r will be used in the following section to calculate the enhancement factor for IR absorption of CO adsorbed on nm-Rh/GC surfaces at solid/gas interfaces. Table 1 shows the data obtained from cyclic vltammetric studies on the electrodeposition of Rh onto GC and the characterization of nm-Rh/GC(n). We can see that with the increase of n from 4 to 50 the d_e is increased from 5.1 to 53.6 nm and the R_r is augmented from 1.09 to 11.57. It may be worth mentioning that the deposition of a rhodium film onto a single-crystal substrate of Au(111) also yielded similar results (i.e., along with the increase of the Rh film thickness, the surface of the film becomes more and more rough).[42]

3. In Situ FTIR Studies of CO Adsorption on nm-Rh/GC Surfaces. 3.1. Spectral Features of Abnormal Infrared Effects (AIREs) of nm-Rh/GC at Solid/Gas Interfaces. In Figure 4, a typical absorption spectrum of CO at saturation coverage on nm-Rh/GC($n = 10$) is shown and compared with a spectrum of CO adsorbed on a massive Rh surface under the same conditions. We observe in both spectra a positive-going band (i.e., an absorption band) centered at 2143 cm^{-1} with P and R lines. This band can be assigned to the IR absorption of gaseous CO. As indicated in the Experimental Section, both adsorbed CO and gaseous CO presented in the solid/gas interface between the Rh thin film (or massive Rh) and the CaF_2 IR window will be investigated. The appearance of gaseous CO bands confirms the existence in the thin cavity of excess CO species, which ensures the saturation adsorption of CO on the nm-Rh/GC and Rh surfaces. Besides this gaseous CO band, two other small positive-going bands at 2032 and 1888 cm^{-1} appear in the spectrum of massive Rh. These two bands are attributed to the IR absorption of linearly bonded (CO_L) and bridge-bonded CO (CO_B), respectively.[30] The integrated intensities (I) of the two bands are 6.0×10^{-3} and 3.5×10^{-3}, and the values of the full width at half-maximum (FWHM) of the two bands are 32 and 44 cm^{-1}, respectively. In the case of CO adsorbed on nm-Rh/GC($n = 10$), the IR absorption of CO_L and CO_B yields negative-going bands around 2050 and 1907 cm^{-1}, whereas the gaseous CO band is still positive-going. The integrated intensities of the CO_L and CO_B bands were measured to be 1.85×10^{-1} and 1.19×10^{-1}, respectively. It is evident that CO adsorbed on a nanostructured Rh thin film gives rise to anti-absorption IR bands, wherein the direction of the bands of CO adsorbates (CO_{ad}) is opposite to the direction of the gaseous CO band. The direction of the IR bands of CO adsorbed on nm-Rh/GC($n = 10$) is also opposite to the direction of the IR bands of CO adsorbed on a massive Rh surface. Apart from the inverting in the direction of the adsorbed CO bands, we can also clearly observe two other important IR features for CO adsorbed on the nm-Rh/GC($n = 10$) surface: (1) significant enhancement of IR absorption, which is at least 1 order of magnitude larger; and (2) an increase in the FWHM of the CO_L and CO_B bands, from 32 to 45 cm^{-1} and from 44 to 57 cm^{-1}, respectively. These results demonstrate that at solid/gas interfaces thin films of Rh exhibit abnormal infrared effects (AIREs) that are similar to those reported previously at solid/liquid interfaces for nanostructured thin films of Pt, Pd, and Ru and their alloys.[1-9]

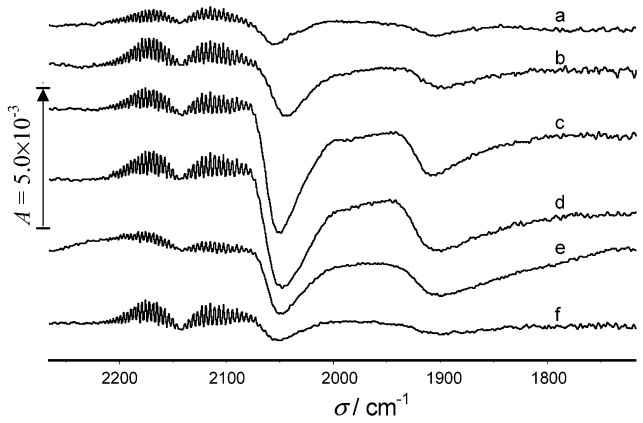

Figure 5. In situ FTIR spectra of gaseous CO and CO adsorbed on nm-Rh/GC(n) with $n = 4$ (a), $n = 7$ (b), $n = 10$ (c), $n = 15$ (d), $n = 30$ (f), and $n = 50$ (g) at solid/gas interfaces.

To determine the enhancement of IR absorption quantitatively, we define an IR enhancement factor (Δ_{IR}) to be equal to the ratio of the IR band intensity of the same amount of CO adsorbed on nm-Rh/GC to that adsorbed on a massive Rh surface:

$$\Delta_{IR} = \frac{1}{R_r} \frac{(I_{COL+COB})_{nm-Rh/GC}/A_{GC}}{(I_{COL+COB})_{Rh}/A_{Rh}} \qquad (6)$$

In eq 6, the term $I_{COL+COB}$ is the sum of the integrated intensities of the CO_L and CO_B bands, which were measured from the spectra of massive Rh and nanostructured thin Rh films under the same experimental conditions. From the IR spectra of Figure 4, we determined Δ_{IR} to be 10.38 on nm-Rh/GC($n = 10$).

3.2. Influence of Rh Film Thickness on the Enhancement of IR Absorption of CO_{ad}. As stated previously, the Rh thin film is a kind of 2D nanomaterial, and the thickness of the film is an important size parameter for this nanometer-scale thin film. It is thus interesting to investigate systematically the influence of the thickness of the Rh thin film on the AIREs. A series of spectra of gaseous CO in the thin cavity and of CO adsorbed on nm-Rh/GC of different Rh film thicknesses are displayed in Figure 5. We can observe in all spectra the positive-going gaseous CO band centered at 2143 cm^{-1} with P and R lines and the negative-going CO_L and CO_B bands at around 2050 and 1900 cm^{-1}, respectively, for adsorbed CO. It is worthwhile to note that the centers of the CO_L and CO_B bands shift slightly

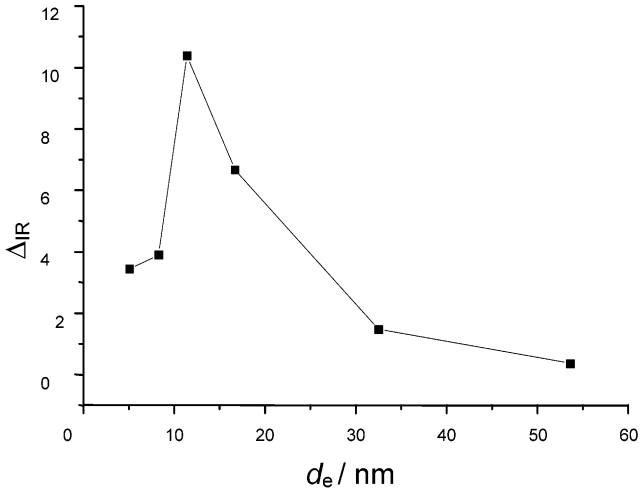

Figure 6. Variation of Δ_{IR} with d_e for CO adsorbed on nm-Rh/GC surfaces at solid/gas interfaces.

TABLE 2: Integrated Intensity of CO_L and CO_B IR Bands ($I_{COL+COB}$) and Δ_{IR} of nm-Rh/GC(n) for Different Values of n

Rh materials	massive Rh	nm-Rh/GC(n), $n = 4$	$n = 7$	$n = 10$	$n = 15$	$n = 30$	$n = 50$
$I_{COL+COB}$	0.0095	0.0358	0.1130	0.3055	0.2990	0.1232	0.0403
Δ_{IR}	1.00	3.45	3.90	10.38	6.68	1.48	0.36

with the variation of the thickness of the Rh thin film. The results in Figure 5 demonstrate that the features of the AIREs are maintained in all spectra (i.e., the inversion of the direction of the CO_{ad} bands, the enhancement of IR absorption, and the increase in the FWHM). It is also interesting to observe significant changes in the enhancement of the IR absorption of CO_{ad} with the variation in the Rh film thickness. Quantitative results obtained from the spectra in Figure 5 are listed in Table 2. We can see that, although the Rh thin films of different thicknesses (except the nm-Rh/GC($n = 50$)) all give rise to an enhancement of the IR absorption of CO_{ad}, the Δ_{IR} varies with the increase of the Rh film thickness. Following the increase of n, both the CO_L and CO_B bands first increase in intensity then decrease synchronously. Δ_{IR} increases at first, when n is less than 10, then decreases for larger n. The maximum value of Δ_{IR} was measured to be 10.38 on the nm-Rh/GC($n = 10$) corresponding to a Rh film thickness of $d_e = 11.4$ nm (or $d_m = 79$ nm). The variation of the enhancement factor Δ_{IR} versus d_e is plotted in Figure 6; it shows an asymmetric volcano curve that is similar to that observed for CO adsorption on nanostructured Rh films at solid/liquid interfaces.[43] Our results show that the AIREs are independent of the medium surrounding the CO/film system (i.e., the AIREs of nanostructured thin film material are always present when the medium surrounding the CO/film system is changed from gaseous CO at solid/gas interfaces to solid/liquid interfaces for the present solvent molecules and ions).

It may be worthwhile to point out that, in the current studies, the saturation adsorption of CO on both massive Rh and nm-Rh/GC(n) surfaces was achieved under conditions in which excess gaseous CO is always present at the solid/gas interfaces during IR measurements. The saturation coverage of CO adsorption on Rh single-crystal planes in an ultrahigh vacuum environment was determined to be 0.75 on both Rh(111)[44] and Rh(100)[45] and 1.0 on Rh(110).[46] We observed from Figure 3 that the features of cyclic voltammograms recorded on all nm-Rh/GC(n) electrodes are similar to those of cyclic voltammogram of the massive Rh electrode, which may imply that the nm-Rh/GC(n) surfaces behave as a polycrystalline Rh. Therefore, the saturation coverage of CO adsorbed on all nm-Rh/GC(n) surfaces may be close to that on massive Rh and may be larger than 0.75. As a consequence, the values of Δ_{IR} listed in Table 2 and plotted in Figure 6 are representative of the degrees of enhancement of IR absorption of CO adsorbed on nanostructured Rh films of different thickness.

As we have stated in the Introduction, the enhancement of IR absorption and the increase in the FWHM of IR bands of adsorbates are both presented in the AIREs and the SEIRA,[10−12,47] and the difference in the IR features of AIREs and SEIRA consists mainly of the inversion of direction of the IR bands of adsorbates. The present results suggest that the nonlinear optical phenomenon of the AIREs is related mainly to the particular properties of the thin film and the nanometer size (the film thickness). We have reported recently that the individually separated Pd nanoparticles confined in supercages of Y zeolites produce exclusively an enhancement of IR absorption and an increase in the FWHM.[48,49] The Rh film prepared by electrochemical deposition under cyclic voltammetric conditions is grown two-dimensionally and exhibits a particular layer structure in which the Rh nanoparticles are connected to each other. This is obviously different from the island structure that initiates the SEIRA.[12,47] The continuously grown Rh film with layer structure can induce a collective interaction of CO adsorbates with nanocrystallites that compose the thin film. Such collective interaction may be one of the origins of the inversion of the direction of the IR bands of adsorbates. It is evident that to understand the origins of the AIREs, further studies involving not only experimental approaches but also theoretical analysis would be worthwhile.

Conclusions

Nanometer thin films of Rh were prepared by electrodeposition under cyclic voltammetric conditions. STM studies revealed that the thin films supported on glassy carbon substrates are composed of layered Rh crystallites and that the electrodeposited Rh atoms are packed in a different way in the thin film compared to those atoms in massive Rh metal. In situ FTIR spectroscopic studies demonstrated that the thin nanostructured Rh films exhibit abnormal infrared effects (AIREs) for CO adsorption at gas/solid interfaces (i.e., an inverting of the direction of IR bands of CO adsorbates, a significant enhancement of IR absorption of CO adsorbed on the film, and an increase in the FWHM of adsorbed CO bands). The inversion in the direction and the increase in the FWHM of CO bands is observed in spectra of Rh thin films of different thicknesses, whereas the enhancement of the IR absorption depends strongly on the film thickness. The enhancement factor shows an asymmetric volcano-type variation. The maximum enhancement of IR absorption was measured to be 10.38 for CO adsorbed on the nm-Rh/GC($n = 10$) corresponding to an Rh film thickness of 79 nm (or $d_e = 11.4$ nm). The present study illustrates further that the AIREs are general phenomena exhibited by nanostructured thin-film materials not only at solid/liquid interfaces but also at solid/gas interfaces.

Acknowledgment. The present study was supported by grants from the National Natural Science Foundation of China (NSFC) and the State Education Ministry of China.

References and Notes

(1) Lu, G.-Q.; Sun, S.-G.; Chen, S.-P.; Li, N.-H.; Yang, Y.-Y.; Tian, Z.-W. In *Electrode Processes VI*; Wieckowski, A., Itaya, K., Eds.; The Electrochemical Society, Inc., 1996, *PV 96−98*, 136.

(2) Lu, G.-Q.; Sun, S.-G.; Chen, S.-P.; Cai, L.-R. *J. Electroanal. Chem.* **1997**, *421*, 19.
(3) Lu, G.-Q.; Sun, S.-G.; Chen, S.-P.; Cai, L.-R.; Tian, Z.-W. *Chem. J. Chin. Univ.* **1997**, *18*, 1491.
(4) Cai, L.-R.; Sun, S.-G.; Xia, S.-Q.; Chen, F.; Zheng, M.-S.; Chen, S.-P.; Lu, G.-Q. *Acta Phys.-Chim. Sin.* **1999**, *15*, 1023.
(5) Lu, G.-Q.; Cai, L.-R.; Sun, S.-G.; He, J.-X. *Chin. Sci. Bull.* **1999**, *44*, 1470.
(6) Lu, G.-Q.; Sun, S.-G.; Cai, L.-R.; Chen, S.-P.; Tian, Z.-W.; Shiu, K.-K. *Langmuir* **2000,** *16*, 778.
(7) Zheng, M.-S.; Sun, S.-G. *J. Electroanal. Chem.* **2001**, *500*, 223.
(8) Zheng, M.-S.; Sun, S.-G.; Chen, S.-P. *J. Appl. Electrochem.* **2001**, *31*, 749.
(9) Chen, Z.; Sun, S.-G.; Zhou, Z.-Y.; Ding, N. *Chin. Sci. Bull.* **2001**, *46*, 1439.
(10) Hartstein, A.; Kirtly, J. R.; Tsang, J. C. *Phys. Rev. Lett.* **1980**, *45*, 201.
(11) Osawa, M.; Ikeda, M. *J. Phys. Chem.* **1991**, *95*, 9914.
(12) Sun, S.-G.; Cai, W.-B.; Wan, L.-J.; Osawa, M. *J. Phys. Chem. B* **1999**, *103*, 2460.
(13) Ortiz, R.; Cuesta, A.; Marquez, O. P.; Marguez, J.; Meadez, J. A.; Gutiérrez, C. *J. Electroanal. Chem.* **1999**, *465*, 234.
(14) Orazco, G.; Gutirrez, C. *J. Electroanal. Chem.* **1999**, *484*, 64.
(15) Bjerke, A. E.; Griffiths, P. R.; Theiss, W. *Anal. Chem.* **1999**, *71*, 1967.
(16) Ukitu, Y.; Kameoka, S.; Miyadera, T. *Appl. Catal., B* **1998**, *18*, 273
(17) Basile, F.; Fornasari, G.; Poluzzi, E.; Vaccari, A. *Appl. Clay Sci.* **1998**, *13*, 329.
(18) Yates, J. T.; Thiel, P. A.; Weinberg, W. H. *Surf. Sci.* **1979**, *82*, 45.
(19) Rabinowitz, H. N.; Tauster, S. J.; Heck, R. M. *Appl. Catal., A* **2001**, *212*, 215.
(20) Nibbelke, R. H.; Nievergeld, A. J. L.; Hoebink, J. H. B. J.; Marin, G. B. *Appl. Catal., B* **1998**, *19*, 245
(21) Jiang, Y. Z.; Xue, S. *J. Organomet. Chem.* **1997**, *586*, 159.
(22) Kunimatsu, K.; Lezna, R. O.; Enyo, M. *J. Eletroanal. Chem.* **1989**, *258*, 115.
(23) Yau, S.-L.; Gao, X.; Chang, S.-C.; Schardt, B. C.; Weaver, M. J. *J. Am. Chem. Soc.* **1991**, *113*, 6049.
(24) Chang, S.-C.; Weaver, M. J. *Surf. Sci.* **1990**, *238*, 142.
(25) Chang, S.-C.; Weaver, M. J. *J. Electroanal. Chem.* **1990**, *285*, 263.
(26) Gao, X.; Chang, S.-C.; Jiang, X.; Hamelin, A.; Weaver, M. J. *J. Vac. Sci. Technol., A* **1992**, *10*, 2927.
(27) Van Hove, M. A.; Koestner, R. J.; Frost, J. C.; Somorjai, G. A. *Surf. Sci.* **1983**, *129*, 482.
(28) Gierer, M.; Barbieri, A.; Van Hove, M. A.; Somorjai, G. A. *Surf. Sci.* **1997**, *391*, 176.
(29) Gerney, B. A.; Richter, L. J.; Villarrubia, J. S.; Ho, W. *J. Chem. Phys.* **1987**, *87*, 6710.
(30) Leung, L.-W. H.; He, J.-W.; Goodman, D. W. *J. Chem. Phys.* **1990**, *93*, 8328.
(31) Leung, L.-W. H.; Goodman, D. W. *Langmuir* **1991**, *7*, 493
(32) Weimer, J. J.; Loboda-Cackovic, J.; Block, J. H. *J. Vac. Sci. Technol., A* **1990**, *8*, 2543.
(33) Lin, W.-F.; Sun, S.-G. *Electrochim. Acta* **1996**, *41*, 803.
(34) Chen, T.-Q.; Zheng, Y.-L.; Chen, Y.; Xin, Q.; Ying, P.-L.; Guo, X.-X. *Chin. J. Catal.* **1991**, *12*, 1.
(35) Frank, M.; Kühnemuth, R.; Baumer, M.; Freund, H.-J. *Surf. Sci.* **1999**, *427*, 288.
(36) Rice, C. A.; Worley, S. D.; Curtis, C. W.; Guin, J. A.; Tarrer, A. R. *J. Chem. Phys.* **1981**, *74*, 6487.
(37) Zaki, M. I.; Kunzmann, G.; Gates, B. C.; Knozinger, H. *J. Phys. Chem.* **1987**, *91*, 1486.
(38) Aribb, M.; Zhang, B.; Lazarov, V.; Stoychev, D.; Milchev, A.; Buess-Herman, C. *J. Electroanal. Chem.* **2001**, *510*, 67.
(39) Sun, S.-G. In *Electrocatalysis*; Lipkowski, J., Ross, P. N., Eds.; Frontiers of Electrochemistry; Wiley-VCH: New York, 1998; Vol. 4, Chapter 6.
(40) Pletcher, D.; Urbina, R. I. *J. Electroanal. Chem.* **1997**, *421*, 145
(41) Wasa, K.; Hayakawa, S. *Handbook of Sputter Deposition Technology: Principles, Technology, and Applications;* Noyes Publications: Park Ridge, NJ, 1992; pp 1−9.
(42) Kibler, L. A.; Kleinert, M.; Kolb, D. M. *J. Electroanal. Chem.* **1999**, *467*, 249.
(43) Lin, W.-G.; Sun, S.-G.; Chen, S.-P.; Wang, H.-C. *Abstracts of The International Conference on Electrified Interfaces* (ninth in a series of nontraditional methods), Wolfville, Nova Scotia, 2001; p 20.
(44) Gerney, B. A.; Richter, L. J.; Villarrubia, J. S.; Ho, W. *J. Chem. Phys.* **1987**, *87*, 6710.
(45) Leung, L.-W.; He, J.-W.; Goodman, D. W. *J. Chem. Phys.* **1990**, *93*, 8328.
(46) Weimer, J. J.; Loboda-Cackovic, J.; Block, J. H. *J. Vac. Sci. Technol., A* **1990**, *8*, 2543.
(47) Nishikawa, Y.; Fujiwara, K.; Ataka, K.-I.; Osawa, M. *Anal. Chem.* **1993**, *65*, 556.
(48) Jiang, Y.-X.; Sun, S.-G.; Ding, N. *Chem. Phys. Lett.*, **2001**, *344*, 463.
(49) Jiang, Y.-X.; Sun, S.-G.; Chen, S.-P.; Ding, N. *Chem. J. Chin. Univ.* **2001**, *11*, 1860.